An echelon-based single shot optical and terahertz Kerr effect spectrometer

View Online   Export Citation   CrossMark

Griffin Mead,[1] Ikufumi Katayama,[2] Jun Takeda,[2] (iD) and Geoffrey A. Blake[1,3,a] (iD)

AFFILIATIONS

[1] Division of Chemistry and Chemical Engineering, California Institute of Technology, Pasadena, California 91125, USA
[2] Department of Physics, Graduate School of Engineering, Yokohama National University, Yokohama 240-8501, Japan
[3] Division of Geological and Planetary Sciences, California Institute of Technology, Pasadena, California 91125, USA

[a] Author to whom correspondence should be addressed: gab@gps.caltech.edu

ABSTRACT

We report on the design and performance of an echelon-based single shot visible/near-infrared spectrometer with adequate sensitivity to measure the nonlinear optical and terahertz Kerr effects in neat molecular liquids at room temperature. Useful molecular information spanning tens of picoseconds can be measured in just a few milliseconds, and the signal-to-noise performance scales favorably with respect to the standard stage scan technique. These results demonstrate the viability of stage-free nonlinear Kerr effect measurements and provide a route for improvements to the speed of future multidimensional Kerr effect studies.

Published under license by AIP Publishing. https://doi.org/10.1063/1.5088377

I. INTRODUCTION

Direct probes of ultrafast molecular dynamics in liquids are of great interest to both experimentalists and theorists seeking to understand fundamental properties of chemical dynamics and energy transfer. Optical and terahertz Kerr effect (OKE/TKE) spectroscopies are particularly useful in this pursuit, offering subpicosecond resolution of a liquid's response to a nonlinear perturbation.[1–3] While easily performed along one time dimension, Kerr effect spectroscopy can be extended to multiple time (frequency) dimensions, revealing fundamental couplings between low energy vibrational and librational modes.[4,5] One root limitation in the speed of OKE/TKE data acquisition is the need to use motorized delay stages which indirectly sample the molecular response in the time domain. While not a large impediment in one-dimensional studies, scanning multiple delay lines in multidimensional experiments rapidly becomes a limiting factor, dictating some compromise between experimental duration, time (frequency) resolution, and sensitivity.

Generally, stage scan limitations have been overcome using specialized gratings, prisms, or spectrally chirped probe pulses. In conjunction with photodiode arrays, these multiplexing techniques can encode many picoseconds of molecular dynamics onto a degree of freedom that can be measured in a single, or a small number of

laser shots. A large body of works have described the application of time-to-frequency, time-to-angle, and time-to-space multiplexing techniques to the linear analog of TKE, terahertz time domain spectroscopy (THz-TDS), and to studying irreversible processes and dynamics in optically excited materials.[6–13] While these techniques are exceedingly useful for probing ultra-fast dynamics of a material's degradation or the profile of a terahertz waveform, we are interested in applying single shot techniques to study Kerr effect phenomena in liquids. Although a few studies have used spectrally chirped probe pulses for single shot OKE measurements of liquids, the application of other single shot techniques is still very much underinvestigated.[14,15]

In this paper, we describe the construction of a single shot apparatus based upon a reflective stair step echelon which maps delay time onto the pixel space of a scientific CMOS (sCMOS) camera array. The design provides a 30 ps measurement window which can be recorded at a 1 kHz acquisition rate. This approach eliminates the use of a stage scan and can measure the OKE and TKE responses of simple liquids in as little as 10 ms (10 laser shots). The echelon technique also avoids fundamental limits in temporal resolution present in time-to-frequency mapping approaches.[13] We demonstrate good agreement between data recorded using the single shot apparatus and the conventional stage scan approach. We further quantify the signal-to-noise scaling of the single shot

approach and find favorable performance relative to using a stage scan. Overall, the performance achieved demonstrates the feasibility of using a reflective stair step echelon to detect nonlinear molecular Kerr effect signals, extending the utility of the reflective echelon technique beyond the well demonstrated linear electro-optic Pockels effect.

II. EXPERIMENTAL SETUP

The laser system used in this work was a 1 kHz Coherent Legend UltraShort Pulse (USP) regenerative amplifier seeded with an 80 MHz Coherent Micra oscillator. The Legend output pulses were split, with 85% of the beam pumping a Light Conversion TOPAS-C traveling-wave optical parametric amplifier (OPA) and a small portion of the remainder used for the detection of Kerr effect signals. The output of the OPA was modulated at 500 Hz with an optical chopper referenced to the 1 kHz regenerative amplifier transistor-transistor logic (TTL) output. Optical Kerr effect (OKE) measurements used an optical pump at 520 nm, produced by mixing the OPA signal beam fundamental at 1500 nm with 800 nm light to generate the sum frequency. Residual 800/1500 nm light was removed with two short pass filters. A neutral density filter was used to further attenuate the 70 μJ optical pump pulse down to ~8 μJ (4 mW average power at 500 Hz modulation) such that the beam would not strike a plasma when focused at the sample. (Plasma generation results in spurious peaks scattered throughout the data which cannot be removed through differential chopping and data processing.) After filtering and attenuation, the pump beam was directed through a half wave plate (HWP) to rotate the horizontally polarized pump beam by 45°. The pump beam was then expanded with a 7.5× magnification off axis parabolic (OAP) mirror telescope and focused onto the sample with a third OAP mirror (Fig. 1). The $1/e^2$ radius of the pump spot at the sample was around 60–70 μm, corresponding to an average power density of 31 W/cm^2 (and an estimated peak power of ≥60 GW/cm^2). A conical hole machined into the rear side of the third OAP mirror provided clearance for the probe beam to pass through with minimal clipping on the sides of the mirror. The exit hole at the OAP front surface was 3 mm in diameter, which negligibly attenuated the 50 mm diameter pump beam.

For terahertz Kerr effect (TKE) measurements, dry nitrogen was used to remove water vapor from the terahertz pump path. The unfiltered 500 μJ (250 mW average power at 500 Hz modulation), 1500 nm TOPAS signal beam output pumped a 6 mm diameter 4-N,N-dimethylamino-4′-N′-methyl-stilbazolium tosylate (DAST) organic crystal THz emitter (DAST, Swiss Terahertz). Residual pump light after the DAST emitter was removed with two THz bandpass filters (QMC Instruments). The THz pump followed the same path as the optical pump, with the addition of a wire grid polarizer (WGP) in the collimated region between OAP 2 and OAP 3 to enforce the 45° pump polarization. The THz pump pulse energy was ~1.5 μJ and was focused by the third OAP to a $1/e^2$ radius of 200 μm at the sample, producing an average power density of 0.6 W/cm^2 (and an estimated peak power exceeding 1 GW/cm^2).

Adapting previously reported designs, the probe beam passed through two reflective telescopes pairs, of which each provided a 8× magnification of the probe beam.[16–18] An iris was also placed

FIG. 1. Diagram of the single shot experimental apparatus. The dashed black squares identify the echelon and post sample probe beam paths that were modified to perform reference stage scans. Dashed green and red squares indicate the optical components used for OKE and TKE measurements. DAST: THz organic crystal emitter, WGP: wire grid polarizer, HWP: half wave plate, Ech: reflective echelon, L1–L4: focusing and imaging lenses, P1, P2: polarizers, QWP: quarter wave plate, LPF: 750 nm long pass filter, Cam: high frame rate camera, PD: Si photo-diode, M: square mirror.

between the two telescope pairs to further improve the final beam profile homogeneity. The probe beam diameter after magnification is 50 mm, and so completely illuminates the 1000 step nickel echelon (step width = 35 μm; step depth = 5 μm). This echelon geometry provides 30 ps of total optical delay, with 30 fs of delay between adjacent "beamlets." The reflected probe beam was then directed off a 50 mm diameter gold mirror before being focused with a Barlow lens combination (L1, L2) through the hole in the third OAP. Immediately before passing through the OAP, the probe beam polarization was conditioned with a 10 000:1 preparatory polarizer (P1) and a quarter wave plate (QWP). The energy of the probe beam at this position was 600 nJ, and focused into a $1/e^2$ radius spot of 73 μm. This corresponds to an average power density of 3.56 W/cm^2, which is several fold larger than the THz average power density. However, the probe power is not contained in a few hundred femtosecond pulse but across 30 ps, which drops the instantaneous power density by several hundredfold (to on the order of 100 MW/cm^2 such that the THz pump power density is much greater than the probe power density).

The orientation of the probe and pump polarizations are aligned such that the measured OKE/TKE signals arise from the anisotropic component of the molecular response function ($R_{aniso} \propto R_{XYXY}$).[19] A traditional optical heterodyne detection scheme was employed to improve the strength of the Kerr effect signals.[20] The fast axis of the QWP was aligned parallel to the P1 polarizer axis, and then the polarizer was slightly detuned (~2°) to introduce a small amount of orthogonally polarized light, which acquires from the QWP a $\pi/2$ phase shift relative to the majority of the probe beam. This small quadrature component acts as a local oscillator during the heterodyne detection of the rotated

probe light. When the local oscillator and signal fields arrive at the camera array, each square law detector (camera pixel) produces a signal proportional to the square of the two incident fields

$$(E_{LO} + E_{sig})^2 = E_{LO}^2 + E_{sig}^2 + 2E_{LO}E_{sig}. \quad (1)$$

This equation is a valid approximation for the single shot measurements, where both the preparatory polarizer detuning angle and induced birefringence in the sample are small. The polarizer angle can be adjusted to ensure that the local oscillator background is always much greater than the Kerr effect response, which ensures the signal is dominated by the term in Eq. (1) that is linearly proportional to E_{sig}. The ultimate limit to the intensity of the local oscillator background is the well depth of the camera pixels. The probe intensity in these experiments corresponded to ≈ 3000 total photon counts per individual unbinned pixel per image (or 10 000 incident photons at a quantum efficiency (QE) of 30% at 800 nm). This probe illumination intensity falls well within the linear photon counting regime of the camera, which has a linearity greater than 99% of the well depth of $30\,000\,e^-$.

In OKE measurements, a 1 mm path length Suprasil QS cuvette contained the sample, while for TKE measurements, a 5×5 mm^2 clear aperture, 1 μm thick silicon nitride window on a 10×10 mm^2 Si substrate (Norcada) was epoxied in place over a glass cuvette with a 6.5 mm diameter hole drilled through one wall, creating an effective path length of 1.5 mm. After interacting with the pumped sample, the probe beam passed through a second 10 000:1 analyzing polarizer (P2) which was crossed at 90° with respect to the fast axis of the QWP. The probe beam then passes through two cylindrical imaging lenses (L3, L4) and a 750 nm long pass filter (LPF) before hitting the camera's sCMOS array. Proper imaging of the echelon surface onto the camera array is absolutely critical for ensuring good quality measurements. The imaging pathway, as well as specific properties and positions of the postechelon Barlow and imaging lenses are presented in the supplementary material.

Data were acquired at 1 kHz using a 10-tap Andor Zyla 5.5 MP camera and the Andor Solis program. Acquisitions were triggered from the regenerative amplifier delay generator, and the exposure time was set to 800 μs so that only a single laser pulse was captured in each image. Chopping the pump beam at 500 Hz allowed for data to be acquired in an on-off manner, which compensated for drift from shot-to-shot fluctuations in beam intensity and pointing. Each data set consisted of 10 000 images (5000 on, 5000 off) that were acquired in 10 s and saved to disk in ".dat" format. A Python script was then used for data processing, and it is included in the supplementary material.

After reshaping the raw data to match the camera dimensions and the number of images acquired, odd and even numbered images were separately coadded. The two data sets (corresponding to pump on and pump off conditions) were then subtracted and normalized by the pump off data set [Eq. (2)],

$$Sig_{O/TKE} = \frac{Sig_{ON} - Sig_{OFF}}{Sig_{OFF}}. \quad (2)$$

As the pump off data set corresponds to E_{LO}^2, the subtraction of the two data sets removes this term. In the experimental case of $E_{LO} \gg E_{sig}$, the resulting signal is now $E_{sig}^2 + 2E_{LO}E_{sig} \approx 2E_{LO}E_{sig}$.

For traditional O/TKE studies using single element photodiodes, the small nonlinear homodyne component can be removed in a few different ways; for example, through performing two measurements with the preparatory polarizer oriented at $\pm\phi$, or through measuring the difference signal recorded by a pair of photodiodes after passing through the sample and a series of postsample polarization optics.[21] By contrast, the simultaneous measurement of E_{LO}^2 in the single shot experiment allows E_{sig} to be numerically calculated using a single data set. Once determined, the heterodyne and homodyne components can be easily separated. For data throughout this study, the very small homodyne component was not removed from the stage scan or echelon data. Instead, we demonstrate the deconstruction of the echelon data into its homodyne and heterodyne components, thus verifying the necessary condition $E_{LO} \gg E_{sig}$ (see the supplementary material).

To improve sensitivity, a 2 pixel horizontal bin and an 8 pixel vertical bin were applied to the 2560×80 pixel subarray of the camera used to acquire data. The 8 pixel vertical binning was aligned parallel to the long axis of the beamlets, and so binning in this direction had no impact on the temporal resolution of the experiment. Coadding along the vertical dimension produced a final data array of 1280×1 values. Accounting for small regions on each side of the camera array which were not illuminated by the probe beam, the 1000 echelon steps were imaged onto an area that horizontally spanned around 1100 $2 \times$ binned pixels (or 2200 total pixels). This slight oversampling of the probe beamlets ensured that the temporal dynamics encoded by the probe were fully resolved by the camera.

Calibrating the pixel-to-time mapping was achieved by translating a delay stage on the probe beam path by 1.4989 mm (10 ps of delay), which resulted in the echelon signal peak shifting along the array by z pixels. (A similar calibration could be easily achieved without a delay line by using a small plate of material with a known thickness and index at 800 nm.) A cross correlation between the t = 0 ps and t = 10 ps data sets calibrated the time axis, and the time resolution per pixel was found to be ~28 fs. This provided a Nyquist-limited bandwidth of 17 THz. Unlike the stage scan technique whose Nyquist-limited bandwidth is easily tuned by changing the sampling rate and speed of the stage scan, the echelon measurements are less flexible due to the finite number of beamlets and detector elements.

While the Nyquist-limited sampling bandwidth set by the echelon imaging onto the sCMOS array is 17 THz, the group velocity dispersion introduced by optics along the probe beam path prior to the sample could reduce the bandwidth by broadening the probe pulse duration. To combat dispersion, the probe beam (initially 51.9 fs after being split from the main Legend beam) makes 6 reflections off of a pair of negative group-velocity dispersion (GVD) mirrors immediately prior to the reflective telescope. This precompensation effectively negates the dispersion introduced by two focusing lenses, the polarizer, the quarter wave plate, and the sample cuvette. The final probe pulse duration immediately before the sample was estimated to be 56.8 fs, which sets the upper practical bandwidth at ~7.7 THz.

III. EXPERIMENTS AND DISCUSSION

A. Kerr effect measurements

The temporal resolution of the system was evaluated using dimethyl sulfoxide (DMSO), which has a OKE signal dominated by

an instantaneous electronic response that follows the square of the optical pump electric field.[15] The stage scan and echelon methods were both used to measure the response of DMSO and produced nearly identical results [Fig. 2(a)].

The full-width at half maximum of the DMSO response measured using the stage scan was 283.8 fs, and that for the echelon data was 285.5 fs. As demonstrated by the difference between the stage scan and echelon data (Diff, offset −0.2), good agreement between the two techniques is achieved, and this confirms that the echelon is imaged properly onto the sCMOS array. Transforming the DMSO data into the frequency domain reveals the echelon data has a signal-to-noise transition around 7.7 THz, with similar results from the stage scan data [Fig. 2(b)].

The small oscillations apparent in the difference between the DMSO data prompted further investigation. To completely remove any molecular orientational response, the empty Suprasil quartz cuvette was directly measured using the two techniques by shifting the focal region from the cuvette volume to the cuvette wall [Fig 2(c)]. While the instantaneous OKE response is similar between the two techniques (FWHM echelon = 299.5 fs, FWHM stage = 280.9 fs), diffraction patterns in the echelon data are visible. The diffraction signal is visible only in the echelon data because the camera provides far greater spatial resolution than a single photodiode. The sinc-like shape of the diffraction pattern is attributed to the probe beam passing through the 3 mm circular aperture in the third

OAP. While such diffraction occurs with radial symmetry in the direction of probe propagation, binning and coadding along the vertical axis results in only diffraction along the horizontal axis of the camera array being resolved.

The aperture diameter responsible for the diffraction artifacts can be calculated using the pixel length, the distance from the OAP surface to camera array, and the magnification factors contributed by the lenses. Applying the standard relationship $\theta_0 = 1.22\lambda/D$ between the photon wavelength, λ, and the angle formed between the diffraction maxima and first minima, θ_0, returns an estimated aperture diameter of 7.2 mm. This is in reasonable agreement with the 3 mm diameter opening in the OAP, especially given that errors can be introduced from estimating the very small angle θ_0 (which is only on the order of ten thousandths of a radian).

While diffraction from the OAP aperture is always present in every image acquired by the camera, probe photons rotated by the nonlinear perturbation in the sample allows an excess number of diffracted photons to accumulate in the pump-on image subset, which subsequently cannot be removed during data processing. Fortunately, these artifacts have a known functional form, and so are amenable to removal by deconvolution techniques. Minimization of the probe beam diameter prior to passage through the OAP aperture would further mitigate these diffraction effects.

Diffraction from passage of the probe beam through the nonlinear aperture created by the pump field in the sample was also considered. However, the pump electric field cross section is Gaussian, and thus, should produce a nonlinearly perturbed region in the sample that also follows a Gaussian distribution. This Gaussian aperture would subsequently yield a Gaussian diffraction pattern which would not produce the oscillatory side-lobes observed in the data. This qualitative observation, coupled with the good agreement between actual and calculated aperture diameters, supports the OAP hole as the source of the weak diffraction artifacts.

Next, the single shot apparatus was used to measure the OKE and TKE responses of carbon disulfide (CS_2). For the single shot experiments, 10 000 images spanning 30 ps of delay were acquired in 10 s, while the stage scan required ∼18 s (18 000 shots) at 250 μm/s to acquire the same 30 ps of data. The third order nonlinear constant of CS_2 is much larger than DMSO (CS_2 Reχ^3 = 93.17 × 10^{-24} m^2/V^2 cf. DMSO Reχ^3 = 14.22 × 10^{-24} m^2/V^2), and the Kerr effect signals are characterized by a slowly decaying molecular orientational response that extends for many picoseconds after the instantaneous electronic response maximum.[22,23] As seen in Figs. 3(a) and 3(b), the OKE and TKE responses of CS_2 are captured with good fidelity using both techniques. Differences in the optical and terahertz Kerr effect responses arise from different contributions from the polarizability and dipole moment operators in the third order response function.[5] The good agreement between techniques is especially promising when the difference in instantaneous probe photon flux between the two methods is considered. While the entire photon flux is contained within the probe pulse duration using the stage scan method, the echelon disperses the same total number of photons over a 30 ps window, reducing the instantaneous photon flux interacting with the sample by roughly two orders of magnitude.
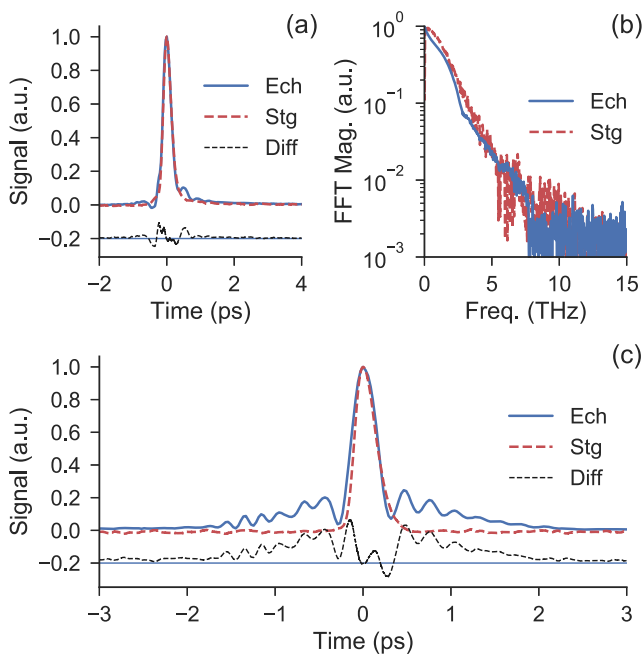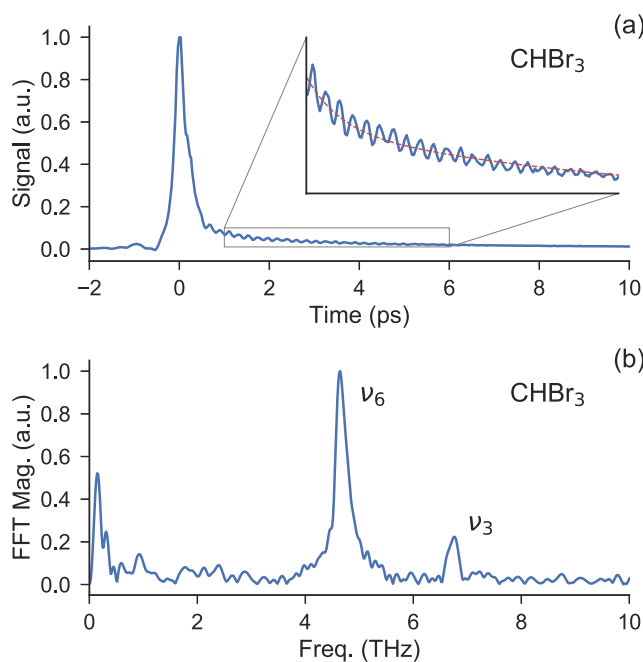

FIG. 2. (a) Comparison of the OKE responses of DMSO measured using the stage scan (Stg) and echelon (Ech) techniques. Diff is the subtraction of the stage scan data from the echelon data, on the same scale and offset −0.2. (b) The FFT of the stage and echelon DMSO data demonstrate similar bandwidths and noise floors. (c) Same as in (a), but the OKE response of the Suprasil quartz cuvette. The diffraction features are clearly apparent around the main OKE response at t = 0 ps.
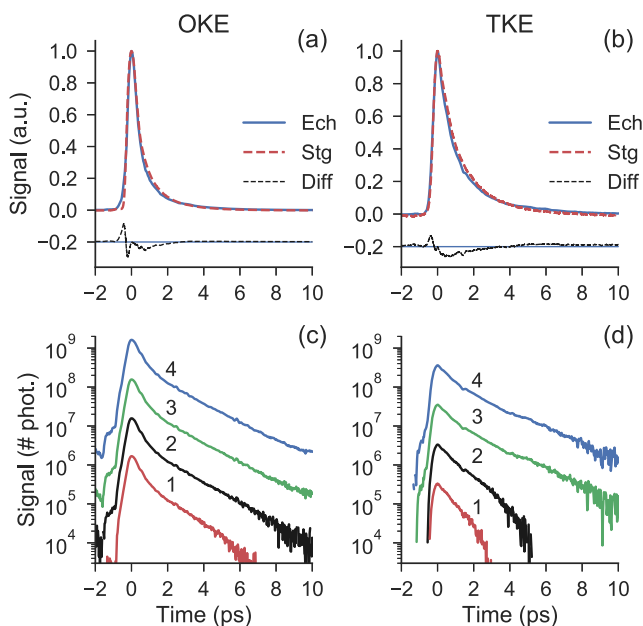
FIG. 3. (a) Linear plots of the CS_2 OKE signal recorded with the echelon (Ech) and stage scan (Stg) techniques as well as the difference between the two (Diff, −0.2). Good agreement between the two techniques is apparent out to t = 10 ps. (b) Similar to (a), but demonstrating the TKE response of CS_2. (c) Evolution of the noise in the single shot CS_2 OKE data across 4 orders of magnitude of sampling (N = 10^x shots, x = 1, 2, 3, 4). (d) The same analysis as in (c), but for the TKE response of CS_2.

FIG. 4. (a) Bromoform OKE response measured using the echelon approach (N = 10 000 shots). The oscillatory molecular coherences are shown in the inset, along with the orientational response fit. (b) The Fourier transform of the fit residual reveals the ν_6 and ν_3 Raman-active modes of bromoform.

To examine the quality of the single shot signal as a function of the number of averages, we extracted from the CS_2 N = 10 000 shot data subsets ranging from N = 5000 to N = 10 shots. In Figs. 3(c) and 3(d), the Kerr effect responses of CS_2 across 4 orders of magnitude of sampling are shown. After 10 shots are acquired the decaying OKE and TKE responses out to several picoseconds are already clearly present. Further sampling extends the decaying response in time and reduces noise. In contrast to the 30 ps of data acquired by the echelon, a stage scan measurement at an equivalent Nyquist-limited bandwidth of 17 THz could only collect around a quarter picosecond of data in 10 ms (optimistically assuming no limitations are imposed by the mechanics of the delay stage).

Finally, we measured the OKE response of bromoform ($CHBr_3$) with the single shot apparatus. Bromoform is a halogenated methane with two low frequency vibrational modes. The full OKE response of bromoform is seen in Fig. 4(a), with the inset highlighting the oscillatory molecular coherences in the data. After detrending a double exponential decay from the data [Fig. 4(a) inset, dashed red line], the residual was Fourier transformed, with two strong features confirming the presence of the molecular modes at 4.66 THz (ν_6, lit. 4.64 THz) and 6.73 THz (ν_3, lit. 6.68 THz), the later of which is at the upper bounds of the practical experimental bandwidth.[24] With the optical pump non-resonant with these two modes, only a nonlinear two-photon Raman process can be responsible for the detection of these features. Similar

molecular coherences were observed in diiodomethane (CH_2I_2), with the 3.65 THz (ν_4, lit. 3.65 THz) mode clearly visible.[25] The diiodomethane data may be found in the supplementary material. Dichloromethane, which has a Raman active mode at 8.5 THz was also measured but no coherences were observed, a finding consistent with the bandwidth limitations imposed by the probe beam duration.

B. Noise performance and sensitivity

The signal-to-noise characteristics of the echelon technique were quantified by calculating the root-mean-square (rms) noise in the OKE response of a series of solvents, and comparing these values to that of stage scan data. The solvents were chosen to span a broad range of χ^3 values, which are directly related to the magnitude of the Kerr response of the liquid. The six liquids measured were acetonitrile ($Re\chi^3$ = 6.61 pm^2/V^2), acetone ($Re\chi^3$ = 10.46 pm^2/V^2), dimethylsulfoxide ($Re\chi^3$ = 14.22 pm^2/V^2), nitrobenzene ($Re\chi^3$ = 21.02 pm^2/V^2), benzene ($Re\chi^3$ = 34.34 pm^2/V^2), and carbon disulfide ($Re\chi^3$ = 93.17 pm^2/V^2).[22]

For each liquid, the mean-corrected percent rms (%σ) of a 3 ps region of the data before the molecular signal was calculated and normalized to the peak of the molecular signal. Comparison data were also acquired using the stage scan method. To keep the information content of the two techniques consistent, the sampling rate of the data acquisition card used for stage scan measurements was adjusted such that the Nyquist-limited bandwidth was 17 THz.

All stage scans collected 30 ps of data, while the stage scan velocity was adjusted to change the number of laser shots acquired in the data sets. The full data sets for each solvent, including comparisons between echelon and stage scan data, as well as extraction of the heterodyne and homodyne components of the echelon data, are included in the supplementary material.

Across the range of weakly to strongly OKE-active liquids, the echelon data had a linear, $1/\sqrt{N}$ relationship between $\log(N)$ and $\log(\%\sigma)$. The rms performance for OKE measurements of acetonitrile and carbon disulfide are shown in Fig. 5(a). The $1/\sqrt{N}$ scaling was constant across 4 orders of sampling magnitude, as demonstrated by the line of best fit. Thus, random Gaussian noise appears to be the predominant noise source in the echelon data. A weaker relationship between the number of shots and the stage scan $\%\sigma$ was found, indicating the data were limited by correlated noise in the measurement and were approaching the noise floor of the stage scan technique for the given experimental parameters.

Next, the rms performance of the CS_2 TKE response was measured using both the echelon and stage scan techniques. The rms behaviors of the two techniques were equivalent in the OKE and TKE experiments, although the TKE response was overall weaker, requiring more measurements to achieve the same rms noise [Fig. 5(b)]. A major cause of the weaker TKE response was the lower terahertz pump energy. For example, at N = 10 000 shots, the measured difference in $\log(\%\sigma)$ between TKE and OKE echelon measurements was 0.88. Given that the Kerr effect signal scales linearly with the pump power (Watts $\propto I = |E^2|$), a difference in $\log(\%\sigma)$ of 1.7 was calculated based upon the ratio of the optical and terahertz pump energies [$1.7 = \log(31\ W/cm^2/0.6\ W/cm^2)$], which agrees well with experiment considering the difficulty in measuring the THz pump power with the same precision as the OKE pump power.

A clear trend was observed in the performance of the two techniques across the range of solvents measured with OKE. In Fig. 5(c), the $\log(\%\sigma)$ after accumulating 10 000 shots was plotted against the logarithm of the third order nonlinear susceptibility χ^3 of each solvent. While solvents with weaker OKE responses tend to reach similar noise floors after 10 000 shots, irrespective of the measurement technique used, the echelon measurements consistently reach lower rms values for even moderately OKE active liquids.

Finally, the sensitivity of the echelon technique was also investigated. For each solvent measured, the total number of signal photons (given by the difference between pump on and pump off data sets) was normalized by the total number of photons in the pump off data set. An identical analysis was performed using a data set with the pump beam blocked, which measures the random error in background photon subtraction for a given probe intensity, and provides a measure of the absolute noise floor of the experiment. As shown in Fig. 5(d), even the weakest OKE response corresponding to a modulation on the order of 0.1% was orders of magnitude larger than the absolute experimental noise floor, which was around 0.001%.

IV. CONCLUSIONS

A single shot, reflective echelon spectrometer design has been shown to acquire accurate OKE and TKE data of simple liquids and has sufficient sensitivity to record tens of picoseconds of molecular signals in as few as 10 laser shots (10 ms). Furthermore, the detection of Raman-active molecular coherences in simple halogenated methanes is especially promising for future applications of the echelon technique to multidimensional nonlinear spectroscopies. Finally, the noise performance of the echelon approach is found to be very competitive to the standard stage scan technique. In sum, these results highlight the feasibility of stage-free nonlinear spectroscopic measurements with orders-of-magnitude faster acquisition times.

As the technique is developed further, a series of questions remain to be explored. In particular, how strongly does the data quality depend upon the camera frame rate and pixel linearity? If data are found to be relatively robust to these parameters, then the methodology outlined above could perform well with a broader set of commercially available cameras, providing a reasonable alternative to motorized stages for performing high resolution nonlinear spectroscopy.

SUPPLEMENTARY MATERIAL

The supplementary material contains further details on the echelon imaging pathway and the data processing code, as well as comparisons of the six solvents' OKE responses measured using stage
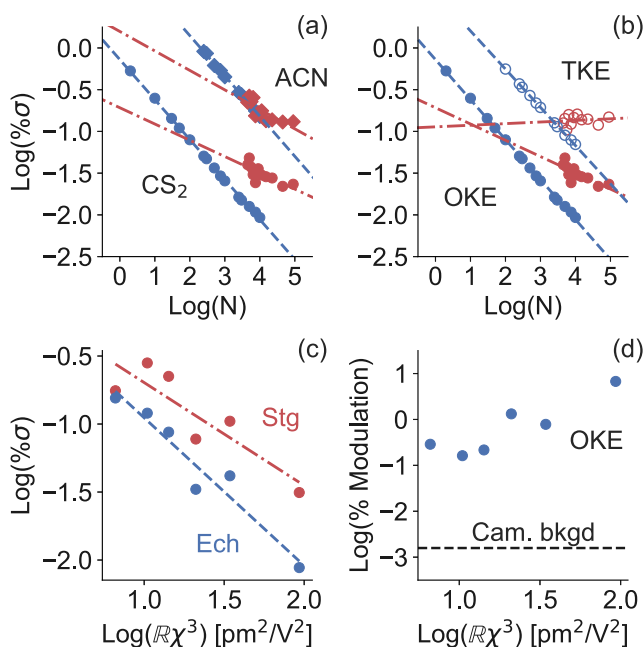
FIG. 5. (a) The rms scaling of OKE signals from two solvents, acetonitrile (ACN, diamonds) and carbon disulfide (CS_2, circles), recorded using the echelon (blue) and stage scan (red) techniques. (b) Comparison between the rms noise performance of the two techniques in the OKE (filled markers) and TKE responses (empty markers) of CS_2. While substantially weaker than OKE, TKE measurements obey similar trends in rms. (c) The OKE rms achieved after N = 10 000 shots for a series of solvents, ranging from weakly to strongly Kerr active (plotted here as small to large χ^3 constants). (d) The ratio of OKE signal photons to background photons (% modulation) observed in the same range of solvents as in (c). The noise floor from random photon fluctuations with no pump present is shown as the dashed horizontal line.

scan and single shot techniques. Also included are brief discussions on separating the homodyne and heterodyne components of the Kerr effect signals and the quadratic scaling of the signal.

ACKNOWLEDGMENTS

REFERENCES

[1]P. Bartolini, A. Taschin, R. Eramo, and R. Torre, "Optical Kerr effect experiments on complex liquids," in *Time-Resolved Spectroscopy in Complex Liquids: An Experimental Perspective* (Springer, 2008), pp. 73–127.

[2]M. C. Hoffmann, N. C. Brandt, H. Y. Hwang, K. L. Yeh, and K. A. Nelson, "Terahertz Kerr effect," Appl. Phys. Lett. **95**, 231105 (2009).

[3]M. A. Allodi, I. A. Finneran, and G. A. Blake, "Nonlinear terahertz coherent excitation of vibrational modes of liquids," J. Chem. Phys. **143**, 234204 (2015).

[4]J. Savolainen, S. Ahmed, and P. Hamm, "Two-dimensional-Raman-terahertz spectroscopy of water," Proc. Natl. Acad. Sci. **110**(51), 20402–20407 (2013).

[5]I. A. Finneran, R. Welsch, M. A. Allodi, T. F. Miller III, and G. A. Blake, "Coherent two-dimensional terahertz-terahertz-Raman spectroscopy," Proc. Natl. Acad. Sci. U. S. A. **113**, 6857–6861 (2016).

[6]P. R. Poulin and K. A. Nelson, "Irreversible organic crystalline chemistry monitored in real time," Science **313**, 1756–1760 (2006).

[7]H. Sakaibara, Y. Ikegaya, I. Katayama, and J. Takeda, "Single-shot time-frequency imaging spectroscopy using an echelon mirror," Opt. Lett. **37**, 1118 (2012).

[8]Y. Minami, H. Yamaki, I. Katayama, and J. Takeda, "Broadband pump-probe imaging spectroscopy applicable to ultrafast single-shot events," Appl. Phys. Express **7**, 022402 (2014).

[9]J. Takeda, W. Oba, Y. Minami, T. Saiki, and I. Katayama, "Ultrafast crystalline-to-amorphous phase transition in Ge2Sb2Te5 chalcogenide alloy thin film using single-shot imaging spectroscopy," Appl. Phys. Lett. **104**, 261903 (2014).

[10]M. Kobayashi, Y. Minami, C. L. Johnson, P. D. Salmans, N. R. Ellsworth, J. Takeda, J. A. Johnson, and I. Katayama, "High-acquisition-rate single-shot pump-probe measurements using time-stretching method," Sci. Rep. **6**, 37614 (2016).

[11]T. Kuribayashi, T. Motoyama, Y. Arashida, I. Katayama, and J. Takeda, "Anharmonic phonon-polariton dynamics in ferroelectric LiNbO$_3$ studied with single-shot pump-probe imaging spectroscopy," J. Appl. Phys. **123**, 174103 (2018).

[12]Y. Minami, Y. Hayashi, J. Takeda, and I. Katayama, "Single-shot measurement of a terahertz electric-field waveform using a reflective echelon mirror," Appl. Phys. Lett. **103**, 51103 (2013).

[13]S. M. Teo, B. K. Ofori-Okai, C. A. Werley, and K. A. Nelson, "Invited article: Single-shot THz detection techniques optimized for multidimensional THz spectroscopy," Rev. Sci. Instrum. **86**, 051301 (2015).

[14]P. Georges, A. Brun, G. Roger, G. Le Saux, and F. Salin, "Single shot measurement of the optical Kerr effect kinetics," Appl. Opt. **27**, 777 (2009).

[15]J. Zhang, S. Liu, T. Yi, X. Wu, Y. Song, B. Zhang, and Q. Zhong, "Ultrafast single-shot measurement of optical Kerr effect based on supercontinuum pulse," Rev. Sci. Instrum. **87**, 43114 (2016).

[16]P. Hello and C. N. Man, "Design of a low-loss off-axis beam expander," Appl. Opt. **35**, 2534 (1996).

[17]L. Yan, X. Wang, J. Si, P. He, F. Chen, J. Zou, and X. Hou, "Multi-frame observation of a single femtosecond laser pulse propagation using an echelon and optical polarigraphy technique," IEEE Photonics Technol. Lett. **25**, 1879–1881 (2013).

[18]G. T. Noe, G. L. Woods, I. Katayama, J. Takeda, D. M. Sullivan, F. Katsutani, Q. Zhang, H. Nojiri, M. C. Hoffmann, F. Sekiguchi, J. A. Horowitz, J. J. Allred, and J. Kono, "Single-shot terahertz time-domain spectroscopy in pulsed high magnetic fields," Opt. Express **24**, 30328 (2016).

[19]M. Khalil, O. Golonzka, N. Demirdöven, C. J. Fecko, and A. Tokmakoff, "Polarization-selective femtosecond Raman spectroscopy of isotropic and anisotropic vibrational dynamics in liquids," Chem. Phys. Lett. **321**, 231–237 (2000).

[20]Q. Zhong and J. T. Fourkas, "Optical Kerr effect spectroscopy of simple liquids," J. Phys. Chem. B **112**, 15529–15539 (2008).

[21]J. Degert, M. Cornet, E. Abraham, and E. Freysz, "Simple and distortion-free optical sampling of terahertz pulses via heterodyne detection schemes," J. Opt. Soc. Am. B **33**, 2045 (2016).

[22]K. Iliopoulos, D. Potamianos, E. Kakkava, P. Aloukos, I. Orfanos, and S. Couris, "Ultrafast third order nonlinearities of organic solvents," Opt. Express **23**, 24171 (2015).

[23]I. A. Heisler, R. R. B. Correia, T. Buckup, S. L. S. Cunha, and N. P. da Silveira, "Time-resolved optical Kerr-effect investigation on CS2/polystyrene mixtures," J. Chem. Phys. **123**, 054509 (2005).

[24]M. Fernández, J. J. López, R. M. Escribano, J. V. García-Ramos, V. Szalay, T. de los Arcos, M. P. Fernández-Liencres, and A. Navarro, "The force field of bromoform: A theoretical and experimental investigation," J. Phys. Chem. **100**, 16058–16065 (2002).

[25]T. J. Johnson, T. Masiello, and S. W. Sharpe, "The quantitative infrared and NIR spectrum of CH$_2$I$_2$ vapor: Vibrational assignments and potential for atmospheric monitoring," Atmos. Chem. Phys. **6**, 2581–2591 (2006).

Supplementary Materials for "An Echelon-based Single Shot Optical and Terahertz Kerr Effect Spectrometer"

Authors: Griffin Mead, Ikufumi Katayama, Jun Takeda, Geoffrey A. Blake[*]

[*]Corresponding author: gab@gps.caltech.edu

Contents of Supplementary Materials:

A. Echelon Imaging

Properly imaging the echelon surface onto the camera array is critical for accurate measurements. The following example demonstrates how the echelon image is propagated along the optical path, and extensively uses the imaging equation

$$\frac{1}{fx} = \frac{1}{Ox} + \frac{1}{Ix} \tag{1}$$

The echelon surface plane is the first object O1 in the imaging pathway (Fig. 1 (a)). Light passing through the first lens L1 (focal length f1 = 200 mm) produces the first image I1 at a distance provided by the imaging equation. This image acts as the second object O2 for the second lens L2. The O2 distance from L2 must account for the 140 mm separation between L1 and L2. The remainder of the imaging pathway follows from this same procedure of propagating images along the optical path.

As the light passes through each lens, the images formed will change size. While the spherical lenses L1 and L2 uniformly change the horizontal and vertical dimensions of the image, the cylindrical lenses L3 and L4 are used to adjust the image magnification along a single axis. The L3 cylindrical lens forms image I3, and de-magnifies the horizontal axis of the echelon image. Similarly, the L4 cylindrical lens de-magnifies the vertical axis. The initial and final dimensions of the echelon object and images are shown in Fig 1 (b). Only a central slice of the final image is acquired by the active sub-array on the camera, as shown (c).
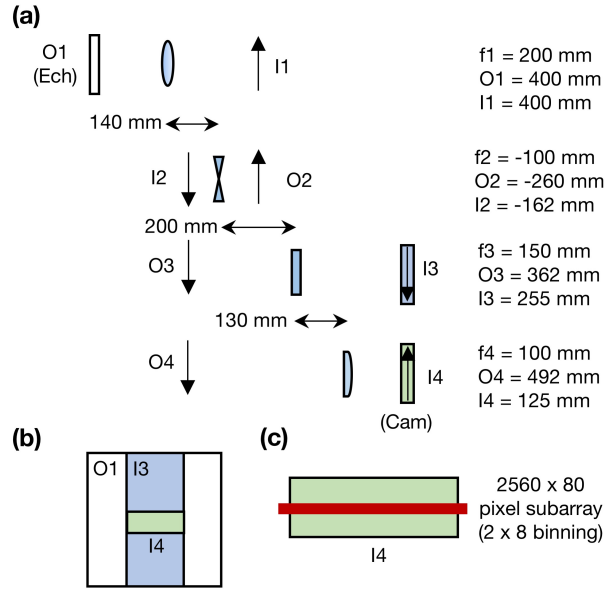
FIG. 1. (a) The location of the echelon image is followed through the optical path between the echelon surface and the camera array. (b) The relative size of the original echelon object (O1) and the images formed after the two cylindrical lenses L3 and L4 (I3 and I4 respectively). (c) A schematic comparison of the size of final image I4 and the active sub-array of the camera used to record the OKE/TKE data. The dimensions of I4 were approximately 14.3 mm wide by 5.1 mm high. The camera subarray used to record data was 16.64 mm wide by 0.52 mm high.

B. Data Processing

The fast frame rate camera can produce large quantities of data quickly; for example, 10 seconds of data from the 1280×10 pixel sub-array with 2×8 binning and 1 kHz acquisition rate produces several hundred megabytes of data. Two data storage and analysis approaches were tested, using ascii ('.asc') and raw ('.dat') data file formats. In Andor Solis, writing .dat files to disk was found to be around 10-20× quicker than storing the data in the .asc format.

Python scripts were used for processing the camera data, and a similar time savings using the .dat file format was evident. With an equivalent series of processing steps, .dat files were analyzed >100× faster than .asc files. The Python script used for .dat file processing is shown below:

```
## bin_reader.py
import numpy as   np
import matplotlib.pyplot as plt
import time


file = 'DIM_10K_.dat' # file name
w = 1280 # array width in pixels, 2x bin
h = 10 # array height in pixels, 8x bin
num = 10000 # number of images acquired


# init. arrays for even and odd image data
odd = np.zeros(w)
even = np.zeros(w)


# start timer
t0 = time.time()


# read in file with appropriate encoding
b =  np.fromfile(file, dtype = np.int32)


t1 = time.time()
c = np.reshape(b, (num, h, w))
```

```python
# sum along the array height
d = np.sum(c, axis=1)


# coadd images
for i in range(num):
    if i % 2 == 0:
        even += d[i,:]
    else:
        odd += d[i,:]


# perform subtraction, normalization
if np.max(even) > np.max(odd):
    diff = (even-odd)/odd
else:
    diff = (odd-even)/even


t2 = time.time()
print 'Read:', np.round(t1-t0, 3)
print 'Process:', np.round(t2-t1, 3)


# save processed data to txt file
np.savetxt('%s_diff.txt' % file, diff)


# plot results
plt.subplot(2,1,1)
plt.plot(even, label='Even')
plt.plot(odd, label='Odd')
plt.xlabel('Pixels (2x bin)')
plt.ylabel('# photons (counts)')
plt.legend(frameon=False)
```

```
plt.subplot(2,1,2)
plt.semilogy(diff, label='Diff')
plt.xlabel('Pixels (2x bin)')
plt.ylabel('Signal (a.u.)')
plt.legend(frameon=False)
plt.show()
plt.close()
```

C. Diiodomethane OKE Response

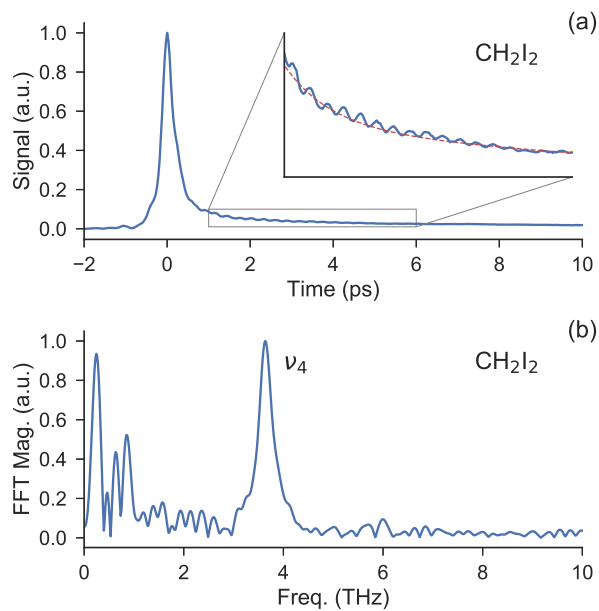The OKE response of diiodomethane (CH_2I_2) was measured using the single shot apparatus, with similar results to bromoform achieved.

FIG. 2. (a) Diiodomethane OKE response measured using the echelon technique (N=10,000 shots). The oscillatory molecular coherences are shown in the inset, along with the orientational response fit. (b) Fourier transform of the fit residual reveals the ν_4 Raman mode at 3.65 THz.

D.   Solvent OKE Responses: Stage vs. Echelon

The six solvents measured using the single shot echelon and stage scan techniques are shown below in Fig 3, with the difference (same scale, offset -0.2) between the two data sets shown to demonstrate the degree of agreement between the two techniques. Some small diffraction arti-facts and irregularities are present in the electronic response regime, which is defined as the few hundred femtosecond region around the signal maximum. The longer picosecond scale molecular orientational responses were found to agree well between the two techniques.
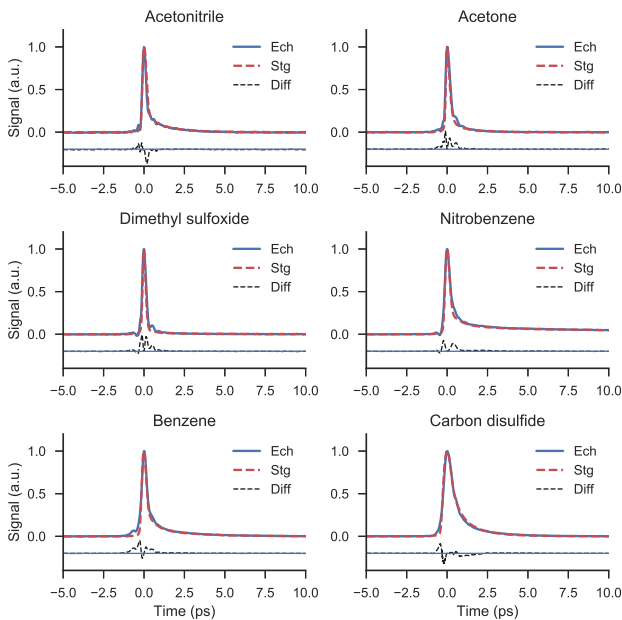
FIG. 3. Comparison plots of the six solvents investigated by OKE, demonstrating the good agreement between the two techniques across a range of response profiles. The echelon data consist of 10,000 laser shots (10 seconds), the stage scan data 45,000 laser shots (45 seconds).

E. Calculation of the Heterodyne and Homodyne Components in the Single Shot OKE Response

The single shot OKE responses of the six solvents measured in this study were decomposed into heterodyne and homodyne components using an algebraic solver written in Python. First, the difference signal Y and background signal E_{LO}^2 were extracted from the N=10,000 shot data set. These two 1280×1 vectors were then used as inputs to a Python symbolic solver which found the roots X to Eq. 4, where $X = E_{sig}$. In Fig 4, the heterodyne and homodyne components are shown for each solvent.
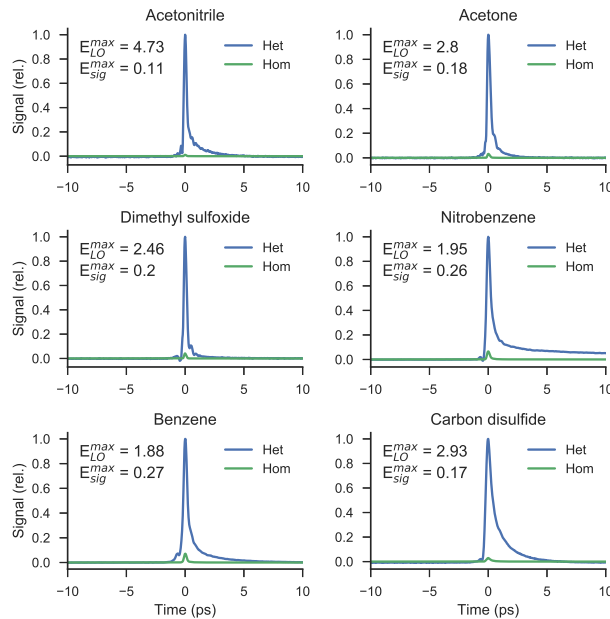
$$Y - X^2 + 2XE_{LO} = 0 \qquad (2)$$

FIG. 4. The heterodyne and homodyne components of the single shot OKE responses of six solvents investigated in this study. The values in the upper left-hand corners specify the maximum relative magnitudes of the calculated E_{LO} and E_{sig} fields, demonstrating the $E_{LO} \gg E_{sig}$ condition for linear heterodyne detection.

F. Quadratic Scaling of OKE Signal

To verify the nonlinear nature of the observed OKE signal, a series of stage scan measurements were performed on CS_2. Neutral density filters were used to attenuate the pump beam power. The relative pump electric field strength of the measurements were calculated by taking the square root of the fractional transmission through each neutral density filter used. Plotting the relative electric field strength against the peak of the CS_2 signal yielded a quadratic relationship, as required for a nonlinear (i.e. $\vec{E}^2_{pump}$ dependent) signal.
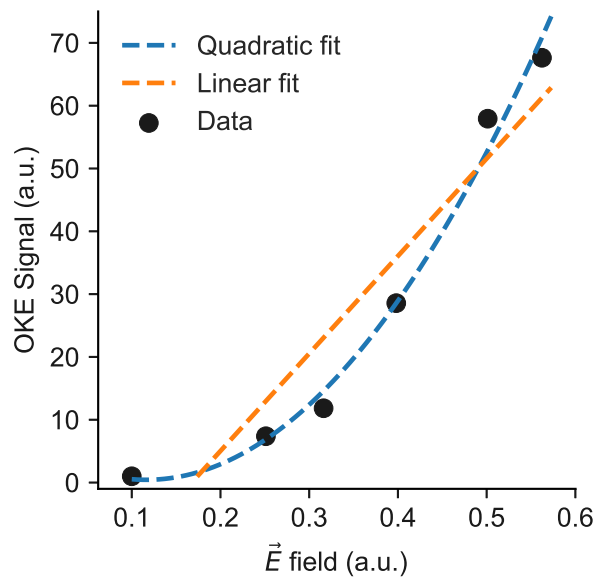

FIG. 5. The peak of the CS_2 OKE signal is plotted as function of the relative pump electric field strength. Data were taken using the stage scan technique, and neutral density filters were used to adjust the intensity of the transmitted pump. A quadratic relationship best fits the data, in contrast to a linear fit, and confirms the nonlinear origin of the OKE signal.